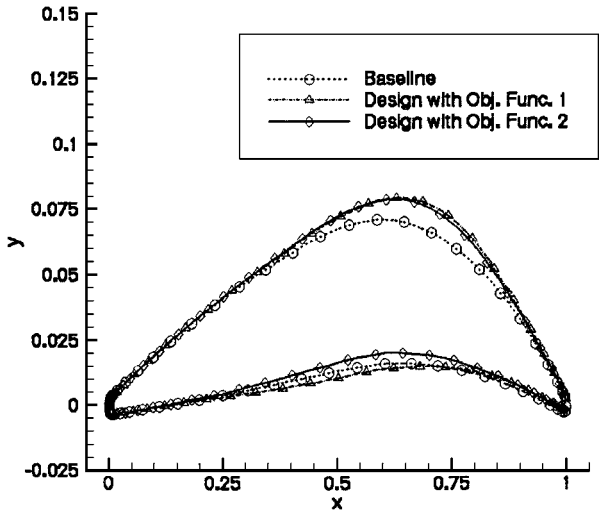

Fig. 1 Geometry of initial and designed blade sections at 50% span.

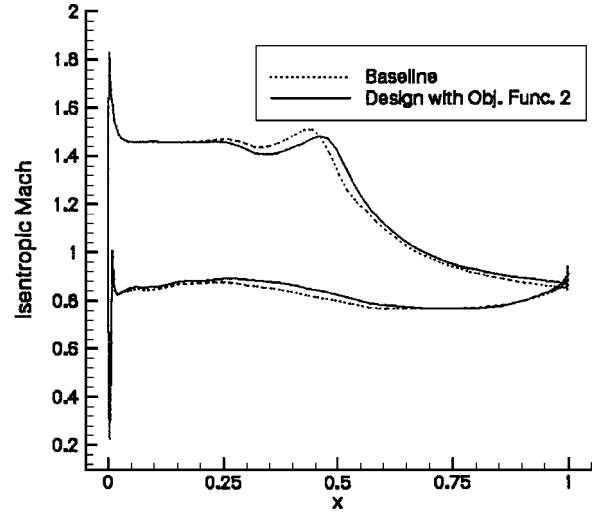

Fig. 2 Isentropic Mach numbers on blade surfaces for blade sections at 50% span.

shock impingement point, it was observed that a reduction in flow separation behind the shock ensued as a result of weakened shock strength.

Conclusions

The flowfield inside transonic compressors involves high-level flow physics and is very sensitive to changes in blade geometry. Therefore, the design of an axial compressor blade requires careful maneuvering through complex nonlinear design space. Numerical optimization is attractive in that constraints can be imposed to prevent ill effects of a design. Constraints, however, limits design space, and in the case of an axial compressor blade design, a constraint on inlet mass flow rate takes too much space away, making optimization extremely difficult to perform. This Note shows that incorporating the constraint into an objective function can improve the design results. Also if needed constraints are related to the objective function in some ways, it would be possible that they all become a part of the objective function while discouraging the design process from moving into certain directions.

The study also shows that the developed design method can improve the adiabatic efficiency of a blade section significantly by reducing the losses from the passage shock and the flow separation. The design method, however, cannot handle three-dimensional effects because it employs quasi-three-dimensional flow physics and did not produce desired design results for the blade section near the hub region. To ascertain the significance of the quasi-three-dimensional design results, constructing and evaluating the performance of three-dimensional blades based on the designed sections will be conducted in the future.

References

[1] Damle, S., Dang, T., Stringham, J., and Razinsky, E., "Practical Use of 3D Inverse Method for Compressor Blade Design," American Society of Mechanical Engineers, ASME Paper 98-GT-115, June 1998.

[2] Wang, Z., Cai, R., Chen, H., and Zhang, D., "A Fully Three-Dimensional Inverse Method for Turbomachinery Blading with Navier–Stokes Equations," American Society of Mechanical Engineers, ASME Paper 98-GT-126, June 1998.

[3] Sorenson, R. L., "A Computer Program to Generate Two-Dimensional Grids About Airfoils and Other Shapes by Use of Poisson's Equation," NASA TM-81198, 1980.

[4] Chima, R. V., "Explicit Multigrid Algorithm for Quasi-Three-Dimensional Viscous Flows in Turbomachinery," *Journal of Propulsion and Power*, Vol. 3, No. 5, 1987, pp. 397–405.

[5] Wilcox, D. C., "Comparison of Two-Equation Turbulence Models for Boundary Layers with Pressure Gradient," *AIAA Journal*, Vol. 31, No. 8, 1993, pp. 1414–1421.

[6] Katsanis, T., and McNally, W. D., "Revised FORTRAN Program for Calculating Velocities and Streamlines on the Hub-Shroud Midchannel Stream Surface of an Axial-, Radial-, and Mixed-Flow Turbomachine or Annular Duct, Part I—User's Manual," NASA TN D-8430, 1977.

[7] "DOT User's Manual," Ver. 3.00, VMA Engineering, Goleta, CA, 1992.

[8] Hicks, R. M., and Henne, P. A., "Wing Design by Numerical Optimization," *Journal of Aircraft*, Vol. 15, No. 7, 1978, pp. 407–412.

R. M. C. So
Associate Editor

Semistructured Grid Generation in Three Dimensions Using a Parabolic Marching Scheme

David S. Thompson* and Bharat K. Soni†
Mississippi State University,
Mississippi State, Mississippi 39762-9627

Introduction

STRUCTURED grids and unstructured meshes have been used successfully to solve a wide range of problems in computational mechanics.[1] Each of these mesh types has advantages and disadvantages that have been well documented in the literature. It seems apparent that meshes consisting of a single-element type cannot simultaneously address the sometimes conflicting requirements of solution accuracy, computational efficiency, and automation of the grid-generation process.

Hybrid grids[2,3] are an attempt to address these requirements by combining elements of both structured grids and unstructured meshes and are attractive because of their flexibility with respect to automation as well as feature resolution through the use of anisotropic elements. Additionally, hybrid grids require significantly fewer elements than unstructured meshes to achieve the same resolution.[2] In a typical hybrid grid, anisotropic prismatic or hexahedral cells are used in regions of the domain near boundaries dominated by large gradients in the field variables. These near-body cells are generated by extrusion of the surface mesh into the domain. Once the mesh is extruded sufficiently far into the domain, tetrahedra are employed to fill the remaining voids. If the extruded mesh

Presented as Paper 2000-1004 at the AIAA 38th Aerospace Sciences Meeting, Reno, NV, 10–13 January 2000; received 29 May 2000; revision received 30 August 2001; accepted for publication 12 October 2001.

*Associate Research Professor, Center for Computational Systems at the Engineering Research Center. Member AIAA.

†Professor of Aerospace Engineering, P.O. Box 9627, Center for Computational Systems at the Engineering Research Center. Senior Member AIAA.

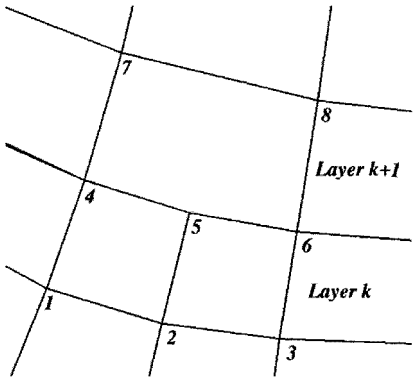

Fig. 1 Semistructured grid topology.

contains quadrilaterals, a pyramidal transition layer must be generated at the interface between the quadrilaterals and the tetrahedra.

In this Note, a novel algorithm to generate a hexahedral-dominant, semistructured grid as a near-body component of a hybrid grid is described. The algorithm uses a parabolic marching scheme[4,5] coupled with a line-deletion/insertion strategy to generate grids that have structure within each layer but might lose local connectivity at the interface between layers. The basics of the approach are discussed, and the algorithm is demonstrated for several example configurations. A detailed description of the algorithm is contained in the full paper found in Ref. 6.

Semistructured Grid Topology

The grid is generated in structured layers starting at the initial data surface, typically the body. Each layer consists of two structured quadrilateral surfaces: the initial data surface for that layer and the surface generated using a parabolic marching algorithm. A line-deletion/insertion algorithm operates at the interface between layers by creating line-deletion/insertion stencils. Using line stencils maintains the structured nature of the grid within layers. This approach produces grid lines that exist in one layer but do not continue into subsequent layers. Traditionally, these grid points have been called hanging nodes.

The node deletion process is illustrated for a two-dimensional grid in Fig. 1. The points 1, 2, and 3 form the initial data surface for layer k. Points 4, 5, and 6 are generated using the parabolic marching algorithm. Points 4, 5, and 6 are not collinear. Based on the deletion/insertion algorithm, it is determined that point 5 should not be used to generate the grid in the next layer $k+1$. Therefore, the initial data surface for layer $k+1$ contains the points 4 and 6 but not point 5. The marching algorithm is then used to generate the surface containing points 7 and 8. However, the cell in layer $k+1$ is actually defined using points 4, 5, 6, 8, and 7, resulting in a five-sided cell even though point 5 was not used to compute points 7 and 8. The extension to three dimensions occurs through the deletion of the line passing through point 5.

The main advantages in using a grid topology of this type with deletion and insertion include 1) improved accuracy in viscous-dominated regions near no-slip boundaries through the use of high-aspect-ratio cells; 2) a more isotropic layer upon which the pyramidal transition layer is generated resulting in a higher-quality tetrahedral mesh; 3) higher-quality grids in regions where grid lines diverge, i.e., near convex corners; and 4) improved efficiency because a dense inner boundary point distribution can be used without the accompanying waste of grid points near the outer boundary. The primary disadvantage of using grids of this type is that the formal order of accuracy of flow solvers developed for arbitrary polyhedra is not well understood. Qualitatively, these grids appear no worse than unstructured and Cartesian meshes from a smoothness perspective. An additional disadvantage specific to the semistructured grids shown here is that the deletion/insertion actions affect the grid distribution throughout an entire layer.

Parabolic Grid Generation

In the parabolic method[4,5] a reference grid is used to make the marching problem well posed. Starting from the initial data surface, two reference grid surfaces are generated. The Poisson grid-generation equations are applied to points on the first surface of the reference grid. This step is equivalent to smoothing the reference grid. The second surface is updated after each iteration of the Poisson grid equations. The second surface of the reference grid is discarded once the desired number of smoothing iterations is complete. The resulting smoothed grid still exhibits many of the characteristics of the reference grid. In this case because the reference grid is generated to be orthogonal, the resulting smoothed grid can be characterized as nearly orthogonal.

Line-Deletion/Insertion Algorithm

The line-deletion/insertion algorithm employed here is based solely on geometrical properties of the grid. It is designed to generate a nearly isotropic outer layer from which a tetrahedral mesh can then be generated. However, there is great flexibility in the design of the deletion/insertion algorithm, and the strategy discussed next is certainly not unique. Assuming that the ζ direction is the marching direction, the procedure used for ξ line deletion will be presented in detail with the extension to η lines by analogy. The line-deletion/insertion scheme described next produces cell faces having four to seven edges, and the resulting volumes might have 6–17 faces. However, for viscous-type grids a majority of the cells (typically greater than 95%) are hexahedra. Any algorithm that generates a structured grid via extrusion could be used with the techniques described next.

Line-Deletion Strategy

A ξ line is tagged for deletion if it meets either of two criteria. The first criterion is based on the average "slenderness" of the cells on a $\xi =$ constant line. A $\xi =$ constant line is marked for deletion if the average value of the ratio of the ζ arc length (g_{33}) to the ξ arc length (g_{11}) is greater than a specified tolerance:

$$\frac{1}{j_{\max}} \sum_{j=1}^{j_{\max}} \left(\sqrt{\frac{g_{33}}{g_{11}}} \right)_j > \alpha_{\text{avg}} \tag{1}$$

where $j_{\max}$ is the number of points on each $\xi =$ constant line. The second criterion is based on a maximum slenderness of the cells on each ξ line. An $\xi =$ constant line is marked for deletion if the value of the ratio of the ξ arc length to the ζ arc length is greater than a specified tolerance at any point on the line or

$$\max_j \left(\sqrt{\frac{g_{33}}{g_{11}}} \right)_j > \alpha_{\max} \tag{2}$$

Note that α_{avg} and $\alpha_{\max}$ are user-specified constants with $\alpha_{\max} > \alpha_{\text{avg}}$.

Because the criteria described in Eqs. (1) and (2) are defined on a line-by-line basis without any information regarding adjacent lines, the deletion/insertion stencil must depend on the information from adjacent lines. In the case of an odd number of contiguous ξ lines selected for deletion, the first line of the group and every other succeeding line of the group are deleted. The case of a single line selected for deletion is trivial. The case of an even number of contiguous ξ lines selected for deletion is treated using a delete two/insert one strategy. For each consecutive pair of lines tagged for deletion, both are deleted and replaced by the line defined by connecting the midpoints between the two lines tagged for deletion. By using a line-deletion algorithm based on cell aspect ratio, lines are deleted as the cell aspect ratio increases as a result of the stretching in the direction normal to the wall.

Line-Insertion Strategy

The criteria used to determine whether a $\xi =$ constant line should be inserted is based on the divergence of the $\xi =$ constant faces of the cell. Unlike the deletion criteria, the insertion criteria apply to a cell face rather than a line. Here, the divergence of a cell face is defined as

$$\Delta = \frac{1}{\sqrt{g_{33}}} \frac{\partial}{\partial \zeta} \left(\sqrt{g_{11}} \right) \tag{3}$$

or, equivalently, the rate of increase of the width (g_{11}) of the cell divided by the height of the cell (g_{33}). In the same manner as the line-deletion algorithm, average and maximum values of the divergence

are used in the algorithm. A surface of $\xi =$ constant and $\zeta =$ constant cell faces is tagged for ξ line insertion if the average divergence exceeds a specified tolerance:

$$\frac{1}{j_{\max}} \sum_{j=1}^{j\max} (\Delta)_j > \beta_{\text{avg}} \tag{4}$$

Similarly, a surface of $\xi =$ constant and $\zeta =$ constant cell faces is tagged for ξ line insertion if the maximum divergence exceeds a specified tolerance:

$$\max_j (\Delta)_j > \beta_{\max} \tag{5}$$

where $\beta_{\max} > \beta_{\text{avg}}$. The line insertion occurs at the midpoints of the cell faces.

Sample Grids

We now include two sample grids to illustrate the general properties of the method. Figure 2 shows the symmetry plane and a spanwise surface for a grid generated around an M6 wing. Figure 3 shows surfaces of a grid generated for an "X-38-like" configuration. In both cases line deletion produces a transition from a relatively dense body grid to a much coarser, more isotropic grid at the boundaries without the clustering of grid lines emanating from concave regions that is characteristic of grids generated using marching methods.

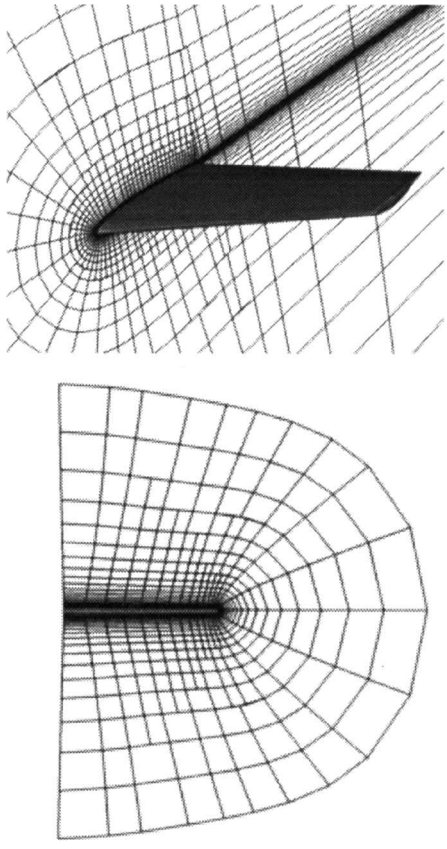

Fig. 2 Symmetry plane and spanwise surface of grid for M6 wing.

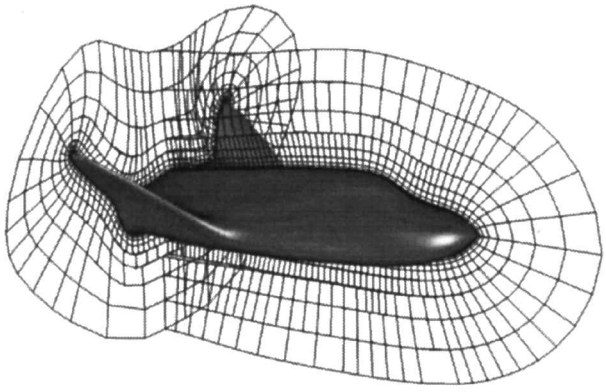

Fig. 3 Symmetry plane and exit surface of grid for X-38-like body.

Conclusions

The capability to generate semistructured, three-dimensional, hexahedral-dominant grids has been demonstrated. The method was shown to generate quality volume grids for surfaces with concave and convex regions. Although the parabolic marching method generates the grid in structured layers, this structure is lost at the interface between layers where a line-deletion/insertion algorithm based on cell aspect ratio and grid line divergence was applied. This strategy is not unique, and great flexibility exists in the definition of the deletion/insertion algorithm.

References

[1] Thompson, J. F., Soni, B. K., and Weatherill, N. P. (eds.), *Handbook of Grid Generation*, CRC Press, Boca Raton, FL, 1998.

[2] Shaw, J. A., "Hybrid Grids," *Handbook of Grid Generation,* edited by J. F. Thompson, B. K. Soni, and N. P. Weatherill, CRC Press, Boca Raton, FL, 1998, pp. 23.1–23.18.

[3] Kallinderis, Y., "Hybrid Grids and Their Applications," *Handbook of Grid Generation,* edited by J. F. Thompson, B. K. Soni, and N. P. Weatherill, CRC Press, Boca Raton, FL, 1998, pp. 25.1–25.18.

[4] Nakamura, S., "Marching Grid Generation Using Parabolic Partial Differential Equations," *Numerical Grid Generation*, edited by J. F. Thompson, Elsevier, New York, 1982, pp. 775–786.

[5] Noack, R. W., and Anderson, D. A., "Solution-Adaptive Grid Generation Using Parabolic Partial Differential Equations," *AIAA Journal*, Vol. 28, No. 6, 1990, pp. 1016–1023.

[6] Thompson, D. S., and Soni, B. K., "Semistructured Grid Generation in Three Dimensions Using a Parabolic Marching Scheme," AIAA Paper 2000-1004, Jan. 2000.

J. Kallinderis
Associate Editor

Evaluation of Finite Element Predictions of Analog Specimen Residual Stress Bondline Failures

David E. Richardson,* Bradley R. Hoskins,†
and Russell A. Crook‡
Thiokol Propulsion, Brigham City, Utah 84302-0707

Introduction

DEPENDING on the bonded system, manufacturing-induced bondline residual stresses can have a significant influence on the integrity of the system. There is a need for accurate and verifiable analytical techniques that can be used in the evaluation of bondline residual stresses. This Note will cover the testing and analyses that have been done with an analog cone residual stress specimen. The goal of this Note is to show that analytical predictions of bondline residual stress failures can be made with accuracy. To show the validity of the analyses, comparisons of the predicted failure times with the actual failure times are made.

This effort was initiated because significant work has been recently conducted to understand the effects of residual stresses on the

Presented as Paper 98-1945 at the AIAA/ASME/ASCE/AHS/ASC 39th Structures, Structural Dynamics, and Materials Conference, Long Beach, CA, 20–23 April 1998; received 7 August 2000; revision received 20 August 2000; accepted for publication 20 August 2000.

* Staff Engineer, Nozzle Design Engineering.
† Senior Engineer, Nondestructive Test Engineering.
‡ Senior Engineer, Adhesives Materials and Processes.